Role of Dispersive Waves in Collisionless Magnetic Reconnection

B. N. Rogers,[1] R. E. Denton,[1] J. F. Drake,[2] and M. A. Shay[2]

[1]*Department of Physics and Astronomy, Dartmouth College, Hanover, New Hampshire 03755*
[2]*Institute for Plasma Research, University of Maryland, College Park, Maryland 20742*

Simulations of collisionless magnetic reconnection show a dramatic enhancement of the nonlinear reconnection rate due to the formation of an open outflow region. We link the formation of this open configuration to dispersive whistler and kinetic Alfvén wave dynamics at small scales. The roles of these two waves are controlled by two dimensionless parameters, which allow us to identify regions of fast and slow reconnection.

Recent studies of collisionless magnetic reconnection, based on both full-particle and two-fluid numerical simulations, have revealed fast rates of reconnection that dramatically exceed those obtained from conventional resistive magnetohydrodynamic (MHD) models [1]. These fast rates of reconnection depend critically on the formation of an open X-line magnetic geometry, in which the width of the outflow layer δ increases with distance from the X-point [2]. At sufficiently large scales where the MHD description becomes valid, these solutions resemble the open X-line configuration analyzed by Petchek [3]. At smaller scales, however, the breakdown of the MHD model leads to a region close to the X-point in the simulations where two-fluid effects dominate. In this region, the electron and ion motions decouple, and the electron flows are observed to scale inversely with the width of the layer [4,5]. This allows the total flux of electrons from the layer $v\delta$ to remain large even as δ becomes very small and leads to a rate of magnetic reconnection that is insensitive to the mechanism which breaks the frozen-in condition [4,6].

Past studies have linked this important property of the electron flows in the non-MHD systems to the Hall term in the generalized Ohm's law [1]. This term introduces the dynamics of whistler and kinetic Alfvén waves into the system, which have phase velocities $v_\phi \propto k$ ($\omega \propto k^2$) that increase with decreasing scale. Here we go beyond past work to show the dispersive character of whistlers and kinetic Alfvén waves also plays the central role in producing the open outflow region which characterizes two-fluid or kinetic reconnection. Specifically, in the MHD case, it is suggested that the acceleration away from the x-line by the standing Alfvén wave, because of the dispersion properties of the wave, leads to the collapse of an open outflow configuration into the macroscopic, elongated current sheet. In contrast, acceleration by the standing whistler or kinetic Alfvén wave in the open outflow configuration, because of the quadratic dispersion character, remains stable and facilitates fast reconnection even in very large systems [2]. We show, based on an analysis of the two-fluid dispersion relation and nonlinear simulations of reconnection, that the dynamics are controlled by two dimensionless parameters,

which measure the strength of the out-of-plane field and the plasma pressure. These parameters allow us to define regions in which the reconnection is fast or slow based on the presence or absence of quadratic waves at small scales.

We first describe the process that causes the reconnection layer to open up in simulations without a strong out-of-plane (guide) magnetic field, such as those of Ref. [1]. Our simulations are based on a collisionless two-fluid model [5] with finite electron inertia. The initial equilibrium [2] is a double current sheet in the (x, y) plane with $\vec{B} = B_x\hat{x} + B_z\hat{z}$, $B_x = B_0\{\tanh[2y/w_0] - \tanh[2(y + L_y/2)/w_0] - 1\}$, and $8\pi p + (B_x^2 + B_z^2) = \text{const}$. We apply periodic boundary conditions and an isothermal equation of state. Reconnection is initiated by a small perturbation. The opening up of the layer occurs in the early nonlinear phase of reconnection. The magnetic separatrix, along with the out-of-plane current and ion flow channel, opens up within a macroscopic X-like region. This can be seen in Fig. 1(a), which shows the out-of-plane current near the magnetic X-point in a simulation with $(L_x, L_y) = (10, 5)d_i$, $d_i = c/\omega_{pi}$, $m_i/m_e = 300$, $w_0 = d_i$, $B_z(t = 0) = 0$, $4\pi n_0(T_e + T_i)/B_{x0}^2 = 1$, and $n_0 = n(y \gg w_0)$ (the scales are in units d_i with $n = n_0$). In the absence of a strong guide field, the opening process is insensitive to both the ion dynamics and electron inertia. Our analysis can therefore be carried out within the framework of the electron MHD (EMHD) model, in which the dynamics can be described by the two components of the magnetic field $\vec{B} = B_z\hat{z} - \hat{z} \times \nabla\psi$:

$$\partial_t B_z + \frac{c}{4\pi ne}[\psi, \nabla^2\psi] = 0, \qquad (1)$$

$$\partial_t \psi + \frac{c}{4\pi ne}[B_z, \psi] = 0, \qquad (2)$$

where $[A, B] = \hat{z} \cdot \nabla A \times \nabla B$ and the electron velocity is $\vec{V}_e = -\vec{J}/ne = [c/(4\pi ne)](\hat{z} \times \nabla B_z + \hat{z}\nabla^2\psi)$. As can be seen from the expression for $\vec{V}_e$, the field B_z [times $c/(4\pi ne)$] is the stream function for the in-plane electron flows. These flows are, in turn, according to Eq. (2), frozen into the in-plane magnetic field. The key to understanding
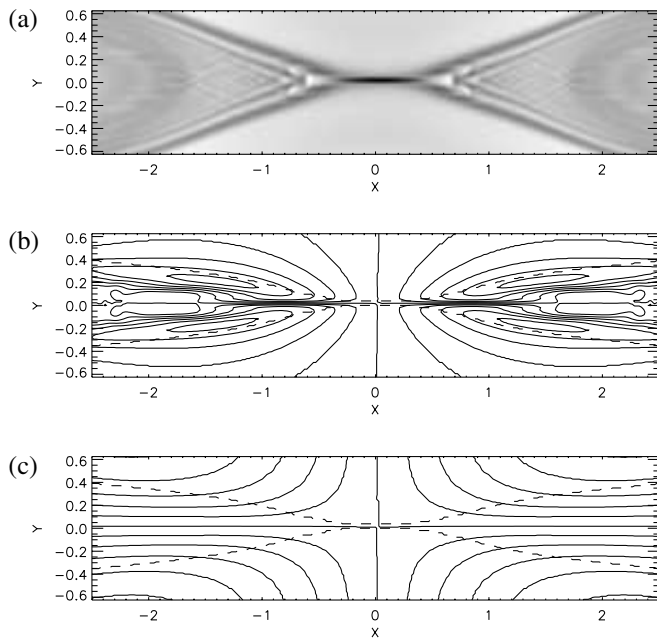
FIG. 1.　(a) J_z; (b) B_z; (c) χ.

why the reconnection layer opens up therefore lies within the structure of B_z.

A contour plot of B_z during the opening-up phase [earlier than Fig. 1(a)] is shown in Fig. 1(b), with the magnetic separatrix shown as the dashed line. The quadrupole structure [7] is caused by parallel gradients of the out-of-plane electron current, which stretch the magnetic field in the out-of-plane direction. These gradients are strongest just downstream of the separatrices and lead to the elongated peaks in Fig. 1(b). Recalling the role of B_z as the electron stream function, the closed contours associated with these extrema represent convective-cell flows. These flows are, in fact, simply the in-plane currents needed to generate B_z. These flows diverge from the horizontal symmetry line downstream as they circle the region of strongest B_z. Because they are frozen into the in-plane magnetic field, they act to rotate the magnetic field lines and drive open the reconnection layer.

Such flows do not occur in an ordinary MHD system without the Hall term. This can be seen by comparing Eqs. (1) and (2) to the analogous equations of reduced MHD (see, e.g., Ref. [8] and references therein):

$$-D_t\nabla^2\phi + [1/(4\pi nm_i)][\psi, \nabla^2\psi] = 0, \qquad (3)$$

$$\partial_t\psi + [\phi, \psi] = 0. \qquad (4)$$

Noting the similarity of Eqs. (1) and (3), one would expect B_z in the EMHD system, for a given profile of ψ, to qualitatively resemble the vorticity $\nabla^2\phi$ in the MHD system. An important difference then arises in Eq. (2), however, in which the vorticitylike quantity B_z convects the in-plane flux rather than the usual velocity potential ϕ, as in Eq. (4). Qualitatively, therefore, EMHD is like MHD except the "vorticity" convects ψ. The impact of this is illustrated

in Fig. 1(c). Given the B_z field of Fig. 1(b), we plot the stream lines (contour lines) of an effective potential χ satisfying $B_z = -\nabla^2\chi$. The stream lines of χ, which would convect the in-plane flux in an MHD-like system, do not exhibit the convective-cell flows associated with B_z that open the layer in the EMHD system.

The essential differences between the MHD and two-fluid systems can also be understood in more physical terms using a simple model, which treats the reconnected field lines downstream of the x-line as a half-wavelength segment of a nonlinear standing wave. Flows which result from the release in the stress of this field line are calculated. Taking δ to be the distance between the separatrices bounding the outflow region, the reversal of B_x across the layer is modeled as $B_x = B_{x0}\sin(ky)$ with $k = \pi/\delta$, where $\delta \sim x$ is assumed to increase with distance from the x-line. We now argue that in the MHD model such an initial open magnetic configuration will collapse with time to form an extended Sweet-Parker layer. The outflow velocity V_x in this standing wave configuration is given by $c_{Ax}\cos(ky)\sin(\omega t)$, $\omega = kc_{Ay}$, $c_{Ay} = B_{y0}/(4\pi m_i n)^{1/2}$, where the amplitude $c_{Ax} = B_{x0}/(4\pi m_i n)^{1/2}$ is the usual outflow velocity based on the "upstream" strength of the magnetic field. In an open x-point geometry close to the x-line, the components of the magnetic field, B_x and B_y, both increase with increasing x [2,9], and thus so does the peak MHD velocity $V_x \sim c_{Ax} \sim B_x$. Steady state conditions are impossible under these circumstances, as can be seen (for example) from Faraday's law evaluated along the center of the outflow region ($y = 0$): $\dot{B}_y = -\partial_x(V_{ex}B_y)$, where in MHD $V_{ex} = V_x$. The increase of $V_{ex}B_y \sim B_xB_y$ with distance x in the MHD case implies $\dot{B}_y < 0$, i.e., a collapse of the layer. (Similar conclusions are reached in Refs. [9,10] following different arguments.) The acceleration by the whistler wave, on the other hand, because of its quadratic dispersion property, is very different. The outflow velocity V_{ex} of the electrons is given by $kd_ic_{Ax}\cos(ky)\sin(\omega t)$, where $\omega = k^2d_ic_{Ay}$ is the whistler frequency. In this case the amplitude of the whistler wave, proportional to kc_{Ax}, in fact decreases with distance downstream from the x-line, consistent with the electron flows in the simulations [2,5] as well as the requirements of steady state behavior (i.e., the constancy of $V_{ex}B_y$). The extra factor of k, which is linked to the quadratic dispersion character of the whistler wave, therefore alters the structure of the electron flow away from the x-line and allows the open X-point magnetic geometry to persist in steady state.

The preceding discussion suggests whistler dynamics play a unique role in mediating fast reconnection, but this is not the case. Essentially the same arguments apply to systems in which the physics of small scales is controlled by kinetic Alfvén waves rather than whistler waves. This is consistent with simulations of reconnection based on the reduced MHD model with finite $\rho_s = c_s/\omega_{ci}$ effects [8,11,12]. Excluding electron inertia, this model is given by Eq. (3) and a modified version of Eq. (4):

$$\partial_t \psi + [\phi - \rho_s^2 \nabla^2 \phi, \psi] = 0. \tag{5}$$

These equations describe the low-frequency ($\omega \ll \omega_{ci}$) dynamics of low-β systems with a strong equilibrium B_z field, and thus by assumption exclude whistler waves. (The conditions under which this assumption is valid are examined below.) The kinetic Alfvén wave, satisfying $\omega = k\rho_s k_\parallel c_A$ for $k\rho_s \gg 1$, is retained through the terms proportional to ρ_s in Eq. (5). The simulations show the addition of these terms cause the reconnection layer to open up and lead to fast rates of reconnection comparable to those observed in configurations without a guide field. The similarity can be quantified. At sub-ρ_s scales where $\rho_s^2 \nabla^2 > 1$, the structure of Eqs. (3) and (5) reduces to that of the EMHD system Eqs. (1) and (2) with the identification $\nabla^2 \phi \leftrightarrow B_z$. The same arguments given above in the EMHD system can therefore also account for fast reconnection in the simulations of Eqs. (3) and (5), with the role of whistler dynamics replaced by the physics of the kinetic Alfvén wave.

Having established that whistler and kinetic Alfvén wave dynamics can play similar roles, we now address the relative contributions of the two. Motivated by our earlier discussion relating standing waves to the acceleration
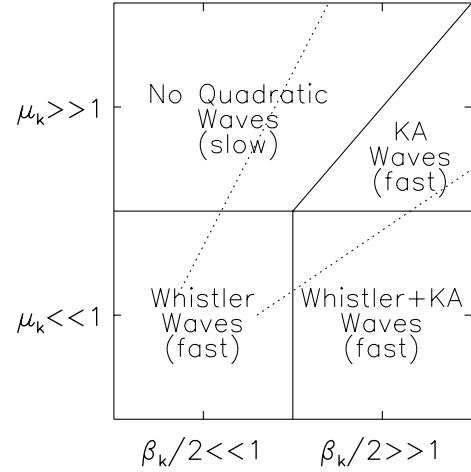

FIG. 2. Parameter space for quadratic waves.

of the plasma away from the x-line, we first approach this question in the context of linear waves with wave vector $\vec{k}$ and a magnetic field at an arbitrary angle with respect to $\vec{k}$. Our analysis is based on the two-fluid model used in the simulations, which in the linear limit yields a cubic dispersion relation in ω^2 (see [13] and references therein):

$$v^6 - \left[\frac{c_{mk}^2}{c_{Ak}^2} + \frac{1}{D}\left(1 + \frac{k^2 d_i^2}{D}\right)\right] v^4 + \frac{1}{D}\left[\frac{c_{mk}^2}{c_{Ak}^2} + \frac{c_s^2}{c_{Ak}^2}\left(1 + \frac{k^2 d_i^2}{D}\right)\right] v^2 - \frac{c_s^2}{D^2 c_{Ak}^2} = 0, \tag{6}$$

where $v = \omega/(kc_{Ak}) = \omega/(k_\parallel c_A)$, $c_{Ak}^2 = B_k^2/(4\pi\rho)$, $B_k = \vec{B} \cdot \vec{k}/k$, $D = 1 + k^2 d_e^2$, $d_e = c/\omega_{pe}$, $c_A^2 = B^2/(4\pi\rho)$, $c_s^2 = (T_e + T_i)/m_i$, $c_{mk}^2 = c_A^2/D + c_s^2$, and $c_m^2 = c_A^2 + c_s^2$. The whistler root, satisfying $v^2 \gg c_m^2/c_{Ak}^2$, can be extracted by balancing the first and second terms in Eq. (6):

$$v^2 \simeq k^2 d_i^2; \qquad \frac{c_m^2}{c_{Ak}^2} \ll k^2 d_i^2 \ll \frac{d_i^2}{d_e^2}. \tag{7}$$

Defining $d_k = d_i c_{Ak}/c_m$, this mode therefore occurs in the scale range $d_e < k^{-1} < d_k$ and requires $d_e^2 \ll d_k^2$, or equivalently $(c_m^2/c_{Ak}^2)(m_e/m_i) \equiv \mu_k \ll 1$. The kinetic Alfvén root, on the other hand, arises in the lower phase velocity regime $1 \ll v^2 \ll c_s^2/c_{Ak}^2$ and therefore requires $c_s^2/c_{Ak}^2 (= \beta_k/2) \gg 1$. This root is obtained by balancing the second and third terms in Eq. (6):

$$v^2 \simeq \frac{c_s^2}{c_m^2} k^2 d_i^2; \quad \frac{c_m^2}{c_s^2} \ll k^2 d_i^2 \ll \min\left\{\frac{d_i^2}{d_e^2}, \frac{c_m^2}{c_{Ak}^2}\right\}. \tag{8}$$

Defining $d_s = d_i c_s/c_m$ ($\simeq \rho_s = c_s/\omega_{ci}$ for $\beta \ll 1$), the kinetic Alfvén root is thus obtained in the scale range $\max\{d_e, d_k\} < k^{-1} < d_s$ and requires $d_s^2 \gg \max\{d_e^2, d_k^2\}$ or $\beta_k/2 \gg \max\{\mu_k, 1\}$. [The requirement $\beta_k \gg 1$ is not apparent in the reduced system, Eqs. (3) and (5). However, since the kinetic Alfvén wave satisfies $\omega \gtrsim kc_{Ak}$, the condition $\omega < \omega_{ci}$ needed for the validity of that model requires $k < \omega_{ci}/c_{Ak}$. Combining this with $k > 1/\rho_s$ leads

to $\beta_k/2 > 1$.] Note the characteristic spatial scales of the kinetic Alfvén wave are necessarily larger than those of the whistler.

In summary, the presence of waves with $v \propto k$ depends on the relationship of three scales: d_s, d_e, and d_k. These yield two independent parameters, $d_s^2/d_k^2 = c_s^2/c_{Ak}^2 = \beta_k/2$ and $d_e^2/d_k^2 = (c_m^2/c_{Ak}^2)(m_e/m_i) \equiv \mu_k$, and four regimes: $\mu_k \ll 1$, $\beta_k/2 \gg 1$, both whistler waves and KA waves are allowed; $\mu_k \ll 1$, $\beta_k/2 \lesssim 1$, whistler waves only; $\mu_k \gtrsim 1$, $\beta_k/2 \gg \mu_k$, kinetic Alfvén waves only; $\mu_k \gtrsim 1$, $\beta_k/2 \lesssim \mu_k$, no quadratic waves. The resulting regimes are shown in Fig. 2.

To interpret the results of reconnection simulations based on this wave analysis, we take $\vec{k} = k\hat{y}$ and $\vec{B} = B_y \hat{y} + B_z \hat{z}$ so that B_k is B_y and B_z is the out-of-plane magnetic field. Unfortunately, B_y is not a parameter of the simulation but develops as a result of reconnection. Generally, B_y will therefore increase with time but will be limited by B_{x0}, the maximum value of the component of $\vec{B}$ which reconnects. The variation of B_y with time defines a trajectory in the μ_y, β_y plane of Fig. 2 given by $\mu_y = m_e/m_i + C\beta_y/2 \simeq C\beta_y/2$, $C = (m_e/m_i)(1 + 2/\beta_z)$. For $C < 1$ (see lower dotted line in Fig. 2), the coupling to dispersive waves will occur even for small values of B_y, while for $C > 1$ (upper dotted line), the coupling to the whistler requires a threshold in B_y to be exceeded before fast reconnection onsets (the
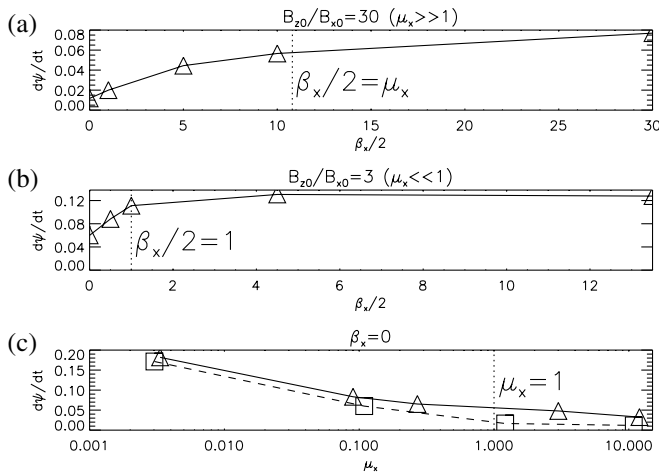

FIG. 3. $\partial_t \psi$ for (a) $B_z/B_x = 30$, (b) $B_z/B_x = 3$, and (c) $\beta = 0$.

FIG. 4. J_z for $B_z/B_x = 30$: (a) $\beta_x/2 = 30$; (b) $\beta_x = 0$.

dotted line enters the lower left quadrant). In any case we presume that at late time $B_y \sim B_{x0}$ and proceed to compare with the simulations by considering $B_k \rightarrow B_{x0}$, $\mu_k \rightarrow \mu_x$, $\beta_k \rightarrow \beta_x$ in Fig. 2, keeping in mind that the replacement of $B_y \rightarrow B_{x0}$ is used only as a convenient parametrization. In the simulations, B_y varies spatially and is in fact typically at most only some fraction of B_{x0} [2].

The two-fluid simulations are carried out with $m_i/m_e = 82.6$ unless otherwise noted and $(L_x, L_y) = (20, 10)d_i$. In the initial equilibrium, $w_0 = d_i$ and the plasma and magnetic pressures are both uniform. We denote the parameters far away from the current sheets as $B_x \approx B_{x0}$, $B_z \approx B_{z0}$, $n \approx n_0$, etc. Figures 3(a) and 3(b) show the nonlinear reconnection rates obtained from the simulations for $B_{z0}/B_{x0} = 30$ [Fig. 3(a)] and $B_{z0}/B_{x0} = 3$ [Fig. 3(b)], as a function of $\beta_x/2 = 4\pi(T_{i0} + T_{e0})n_0/B_{x0}^2$. The corresponding values of $\mu_x = (m_e/m_i)(B_0^2/B_{x0}^2 + \beta_x/2)$ are large in Fig. 3(a) ($\mu_x \simeq 10.9$–11.3) and small in Fig. 3(b) ($\mu_x \simeq 0.12$–0.28). In Fig. 3(b), the whistler/kinetic Alfvén wave regime lies to the right of the dashed line at $\beta_x/2 = 1$ and exhibits the fastest rates of reconnection ($\partial_t \psi \simeq 0.12$). These rates drop by about a factor of 2 ($\partial_t \psi \sim 0.06$) in either the whistler-only regime [Fig. 3(b), left of dashed line] or the kinetic-Alfvén-only regime [Fig. 3(a), right of dashed line]. This decline is reflected in a decrease of the layer opening angle. The essential point, however, is that the reconnection layers in all these cases do open up downstream from the X-point. Figure 4(a), for example, shows results for $\beta_x/2 = 30$, $B_{z0}/B_{x0} = 30$. This is not the case in the simulations at $\beta_x/2 \ll 1$, $\mu_x \gg 1$ [Fig. 3(a), left of dashed line] where the reconnection rate decreases sharply. The layers in these simulations do not open. Figure 4(b) shows results from the most extreme case $\beta_x = 0$, $B_{z0}/B_{x0} = 30$. Finally, Fig. 3(c) shows the reconnection rates at fixed $\beta = 0$ as a function of μ_x for two mass ratios, $m_i/m_e = 82.6$ (squares) and $m_i/m_e = 300$ (triangles). The fact that the two curves are quite similar confirms that μ_x
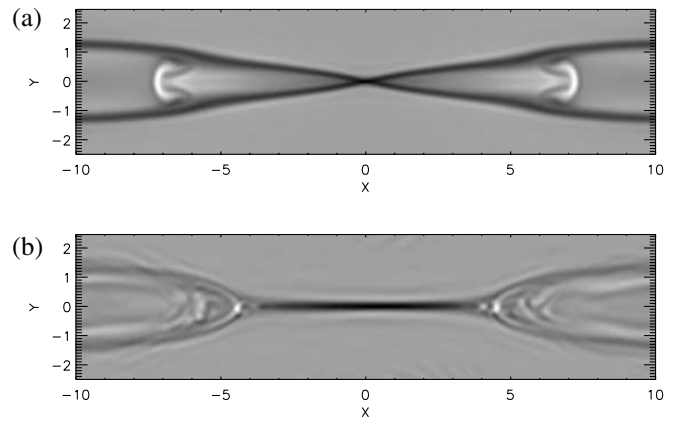
$[= (m_e/m_i)B_z^2/B_x^2$ at $\beta = 0]$, rather than simply [14] B_z/B_x, is the parameter which controls the suppression of the whistler. The dominance of μ_x as the control parameter is consistent with the simulation data presented in Ref. [15].

In summary, fast reconnection in collisionless systems depends on the dynamics of whistler and/or kinetic Alfvén waves at small scales. The condition for whistler dynamics to be present, $B_x^2 > B^2(1 + \beta/2)m_e/m_i$, is satisfied in many systems of physical interest. Assuming this condition is satisfied, the physics at the smallest scales $\sim c/\omega_{pe}$ characteristic of the dissipation region are always governed by whistler waves. If the plasma β is sufficiently high ($\beta \gtrsim B_x^2/B^2$), then kinetic Alfvén dynamics also play a role at somewhat larger scales. Reduced MHD models, which can describe kinetic Alfvén waves but not whistler waves, are therefore inadequate to describe reconnection in such systems. In simulations with very small $B_x^2 \ll B^2 m_e/m_i$ and $\beta \ll m_e/m_i$, no quadratic waves can exist, and the reconnection rate is very small.

[1] J. Birn *et al.*, J. Geophys. Res. **106**, 3715 (2001).
[2] M. Shay *et al.*, Geophys. Res. Lett. **26**, 2163 (1999).
[3] H. Petchek, in *Proceedings of the AAS/NASA Symposium on the Physics of Solar Flares,* edited by W.N. Ness (NASA, Washington, DC, 1964), p. 425.
[4] M. Shay and J. Drake, Geophys. Res. Lett. **25**, 3759 (1998).
[5] M. Shay *et al.*, J. Geophys. Res. **106**, 3759 (2001).
[6] M. Hesse *et al.*, Phys. Plasmas **6**, 1781 (1999).
[7] M. Mandt *et al.*, Geophys. Res. Lett. **21**, 73 (1994).
[8] A. Aydemir, Phys. Fluids B **4**, 3469 (1992).
[9] D. Biskamp, in *Magnetic Reconnection in Plasmas,* edited by M. Haines (Cambridge University Press, Cambridge, 2000), Chap. 6.
[10] R. Kulsrud, Earth Planets Space **53**, 417 (2001).
[11] R. Kleva *et al.*, Phys. Plasmas **2**, 23 (1995).
[12] E. Cafaro *et al.*, Phys. Rev. Lett. **80**, 4430 (1998).
[13] V. Formisano and C. Kennel, J. Plasma Phys. **3**, 55 (1969).
[14] X. Wang *et al.*, J. Geophys. Res. **105**, 27 633 (2000).
[15] D. Biskamp *et al.*, Phys. Plasmas **4**, 1002 (1997).